

Mineral dust and global tropospheric chemistry: Relative roles of photolysis and heterogeneous uptake

Huisheng Bian and Charles S. Zender

Department of Earth System Science, University of California at Irvine

Abstract. We investigate the influence of mineral dust on tropospheric chemistry in the present climate at the global scale. The analysis examines the effects of dust on photolysis and heterogeneous uptake, operating independently and together. In numerical experiments the size-resolved, time-varying mineral dust distribution predicted by the global Dust Entrainment And Deposition (DEAD) model perturbs the gas phase species in a global Chemical Transport Model (UCI CTM). We find that the photolysis perturbation dominates limited regions in the low to middle troposphere, while heterogeneous uptake dominates the rest of atmosphere. Coupling of the photochemical and heterogeneous effects of dust is weak in the global mean but moderate in dusty regions, where coupling is sometimes responsible for more than 20% of local O₃ changes. Ozone and odd-nitrogen concentrations are perturbed in opposite directions by photolysis and heterogeneous chemistry, resulting in a weak net change. However, both processes decrease the concentrations of OH and HO₂. The global mean change due to dust is -0.7% for tropospheric O₃, -11.1% for OH, -5.2% for HO₂, and -3.5% for HNO₃. Large seasonal signals are present near dust source regions. Over the north African region and tropical Atlantic Ocean downwind, OH decreases by -66.8%, six times more than the global mean reduction. Interestingly, net photolysis-induced annual mean O₃ changes are greater in the Southern Hemisphere than in the Northern Hemisphere, where significantly more dust and O₃ precursors reside. In polar regions, O₃ change is dominated by transported O₃ and is not sensitive to local dust concentration. O₃ change due to photolysis depends not only on dust vertical structure, but also on the availability of O₃ precursors. O₃ change due to heterogeneous reactions on dust is sensitive to dust vertical structure, mainly through the influence of temperature on uptake rates.

1. Introduction

¹Aerosols impact the chemical composition of the atmosphere by providing a surface for heterogeneous chemistry, and for light scattering and absorption at photolytic wavelengths. Mineral dust is an important aerosol to consider in atmospheric chemistry because its natural and anthropogenic sources account for one-third to one-half of total

annual aerosol emissions by mass [Penner *et al.*, 2001]. On average, mineral dust contributes more than 60% of total aerosol optical depth in dusty regions, 15% in urban regions, and up to 10% in the remote Southern Hemisphere [Kinne *et al.*, 2003]. Besides seasonal and annual dust variations, dust fluctuates on climatic time scales in both source regions and downwind [e.g., Ram and Koenig, 1997; Kohfeld and Harrison, 2001]. This work focuses on the current annual mean and seasonal cycle of global dust-chemistry interactions.

Convincing evidence that heterogeneous chemistry on

¹Copyright 2003 by the American Geophysical Union.
0148-0227/03/2002JD003143\$09.00

mineral dust significantly alters the concentration of important atmospheric gases has been firmly established in field, lab, and model settings [Zhang *et al.*, 1994; Dentener *et al.*, 1996; Tabazadeh *et al.*, 1998; Zhang and Carmichael, 1999; Goodman *et al.*, 2000; Galy-Lacaus *et al.*, 2002; Underwood *et al.*, 2001; Michel *et al.*, 2002]. Research also shows mineral dust significantly alters atmospheric photochemistry by absorption and scattering in photolytic wavelengths [Dickerson *et al.*, 1997; Jacobson, 1998; He and Carmichael, 1999; Balis *et al.*, 2001; Bian *et al.*, 2003]. These previous three-dimensional Chemical Transport Model (CTM) simulations of the chemical influence of dust focus on the impact of one process (photochemical or heterogeneous) in isolation on atmospheric oxidants. Many of these efforts were conducted on regional spatial scales and/or event-based or synoptic timescales. Recent research on global tropospheric chemistry includes the dust impact through both processes [Martin *et al.*, 2002; Liao *et al.*, 2003] but does not thoroughly analyze or attribute the chemical forcing by dust. In this paper, we use a CTM framework to investigate the chemical alteration of the troposphere by dust through both photolysis rate forcing and heterogeneous uptake. We also highlight the non-linear interaction between dust photolysis rate forcing and heterogeneous uptake to determine the bias that arises from neglecting this interaction.

Our objectives are: (1) Estimate the perturbation by dust to global oxidant distributions due to the coupled effects of photolysis and heterogeneous uptake, (2) Isolate the effect of each process and learn whether there are non-linear interactions between them, (3) Identify regions and seasons where dust has its maximum influence on chemistry and compare these to selected observations, (4) Understand the influence of dust horizontal and vertical distributions on ozone production.

The paper is organized as follows. Section 2 describes the two global models employed. Section 3 presents, in order, the results of the model simulations of the photochemical, heterogeneous uptake, and coupled effects of dust, and concludes with the effects of spatial distribution in selected regions. We discuss our main findings, their uncertainties, and implications for future studies follows in Section 4.

2. Simulation Framework

2.1. CTM description

The UCI CTM [Wild and Akimoto, 2001] includes a detailed tropospheric photochemical scheme which uses the ASAD scheme [Carver *et al.*, 1997] with an implicit solver. The chemical scheme includes complete treatment of inorganic plus methane chemistry and a lumped “family” treatment of hydrocarbon oxidation schemes for the represen-

tative species butane, propane, xylene and isoprene. This tropospheric O₃-NO_x-NMHC chemistry scheme contains 36 species, with 88 chemical reactions and 22 photochemical reactions [Wild and Prather, 2000; Bian and Prather, 2002]. Reaction rates are principally taken from DeMore *et al.* [1997] and from Atkinson *et al.* [1997], with additional rates from [Hough, 1991] and from the Leeds University Master Chemical Mechanism. Photolysis rates are calculated with an on-line treatment of molecular, aerosol, and water and ice cloud absorption and scattering using the Fast-J scheme [Wild *et al.*, 2000; Bian and Prather, 2002]. For use in calculating photolysis rates, stratospheric ozone is taken from the Models and Measurements (M&M) climatology [Park *et al.*, 1999] while tropospheric ozone is taken from the instantaneous CTM values.

The meteorology driving the CTM is provided by the Goddard Institute for Space Studies (GISS) general circulation model version II' (4° × 5°, 9 vertical layers) based on the climatological sea surface temperature of the 1980s. The meteorological fields are supplied every 3 hours and linearly interpolated to the nearest time step. The advection scheme conserves second-order moments and considers not only gradients of tracer concentration but also the curvature in the tracer distribution [Prather, 1986].

Dry deposition is treated with a resistance-in-series scheme based on the surface meteorological properties, vegetation type and species solubility [Jacob *et al.*, 1992; Hanson, 2000]. Wet deposition of soluble species is allowed for during convective transport and in large-scale precipitation using Henry's Law coefficients [Bian, 2001]. Washout in rainfall uses precipitation mass fluxes from the supplied meteorological data and the pH of the water droplets. Evaporation occurring in the lower atmosphere allows these processes to transport soluble trace gases down through the atmosphere rather than removing them entirely.

We map the GEIA inventories of trace species emissions from 1° × 1° resolution to the model grid, preserving the second order moments of the emissions. Additional emissions for CO and biomass burning sources at 4° × 5° resolution are from Wang *et al.* [1998a]. Diurnal variations are provided for industrial and biogenic sources, and seasonal variations are provided for soil emissions, methane, and biomass burning sources. NO from lightning is based on the parameterization of Price and Rind [1992]. The vertical mass flux from the meteorological fields is used to define deep convective events to distribute the NO source. An NO source from aircraft is also included [Baugcum *et al.*, 1996].

The upper boundary for stratospheric ozone is calculated with the Synoz model [McLinden *et al.*, 2000]. The global annual mean flux of ozone from the stratosphere is specified as 475 Tg yr⁻¹ based on observations [Murphy and Fahey,

1994]. Synoz allows the circulation to determine where and when O_3 enters the troposphere. A dynamical tropopause is diagnosed as the 120 ppb isopleth of this synthetic ozone. Below this level, the tropospheric chemistry scheme is applied, and above, a simplified stratospheric scheme is used.

2.2. Mineral Dust

The usefulness of global chemical studies of mineral dust depends, in part, on the fidelity of the simulated dust distribution to observations. The climatological global 3-D dust concentrations used in the UCI CTM are predicted by the mineral Dust Entrainment And Deposition (DEAD) model [Zender *et al.*, 2003]. Predictions from DEAD have been used and evaluated against field measurements in numerous aerosol studies [Rasch *et al.*, 2001; Collins *et al.*, 2001, 2002; Mahowald *et al.*, 2002; Luo *et al.*, 2003; Zender *et al.*, 2003].

DEAD predicts the size-resolved distribution of atmospheric dust in four size bins (0.1–1, 1–2.5, 2.5–5, and 5–10 μm). Mobilization processes include entrainment thresholds, moisture inhibition, drag partitioning, saltation feedback, and erodibility enhancements in sedimentary basins. Dry deposition processes include sedimentation and turbulent mix-out. Nucleation and collision scavenging in both stratiform and convective cloud types are simulated. DEAD simulations of 1994–1998 [Zender *et al.*, 2003] in the NCAR MATCH model [Rasch *et al.*, 1997] at T62 \times L28 resolution were averaged to create global 3-D monthly mean dust concentrations for the UCI CTM. These dust concentrations are then re-gridded to the spatial and temporal resolution of the UCI CTM.

Figure 1 depicts the predicted zonal mean mineral dust extinction [km^{-1}] at 340 nm and horizontal distributions of dust optical thickness in January and July. Strong summertime convection lifts dust into higher atmosphere in July, and spreads more dust into remote region. Dust centers around 10°N in January and shifts north to 20°N in July. The annual mean atmospheric dust burden is 29 mg m^{-2} . The geographic and seasonal variations of dust loading are shown and evaluated in Zender *et al.* [2003] and Luo *et al.* [2003]. These studies show that, in the 1980s and 1990s, DEAD broadly agrees with station observations of mass concentration, mass deposition, optical depth, and satellite-inferred dust distribution. The model captures the seasonal migration of the trans-Atlantic African dust plume and the spring maximum in Asian dust outflow. However, DEAD predicts emissions, burden, and optical depth are significantly (10–50%) less than predicted by Ginoux *et al.* [2001], largely due to differences in wet deposition. DEAD underestimates transport and deposition of East Asian and Australian dust to some regions of the Pacific Ocean. An underestimate of long

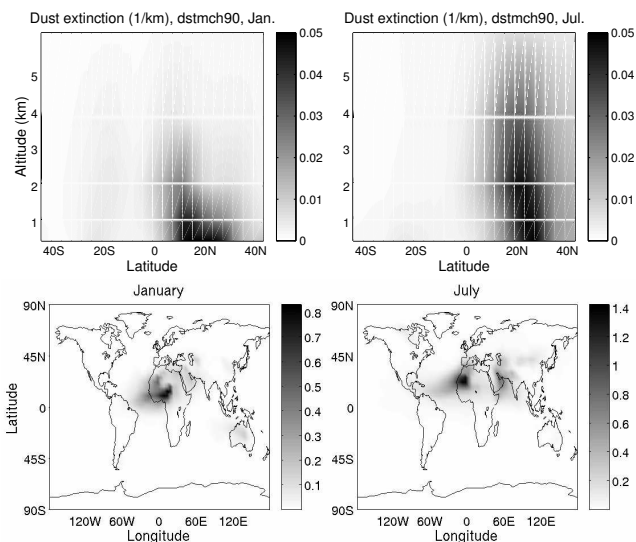


Figure 1. Zonal mean dust extinction [km^{-1}] at 340 nm in January and July (upper panels). Horizontal distributions of dust 340 nm optical thickness in January and July (lower panels).

range transport of particles larger than 3 μm contributes to this common model bias [e.g., Ginoux, 2003; Colarco *et al.*, 2003a].

3. Results and Discussions

The results presented are taken from the final 12 months of CTM simulations of July 1 of year 1 through Jan 31 of year 3. These nineteen month runs include a seven-month spin-up time which allows for most chemically important trace gases, except CH_4 , to reach steady state. Throughout this paper, the influence of dust on atmospheric chemistry is isolated by subtracting the control run (without aerosol) from the perturbation run (with dust) and (for some quantities) dividing by the control run. The species changes reported refer only to tropospheric (i.e., not tropospheric + stratospheric) abundances.

3.1. Effects of Photochemical Forcing

Aerosols manipulate the atmospheric radiance field in such an intricate way that outstanding problems remain in modeling the closure of even the clear sky radiative budget [Valero *et al.*, 2003]. Sokolik *et al.* [2001] review current experimental and theoretical approaches used to quantify the dust radiative effects. They point out that despite recent advances, dust optical properties remain poorly quantified due to limited data and incomplete understanding of relevant

physical and chemical properties. The reader is referred to the existing literature on the sensitivity of photochemistry to plausible ranges of dust optical properties [Liao and Seinfeld, 1998; He and Carmichael, 1999].

The refractive index n is an essential parameter required to derive the optical properties used in photolysis rate calculations. Specifically, Fast-J requires the single scattering albedo and the first 7 coefficients in the Legendre expansion of the scattering phase function for ultraviolet and visible wavelengths (300–600 nm) [Wild *et al.*, 2000; Bian and Prather, 2002]. As in Bian *et al.* [2003], we assume a wavelength independent refractive index, $n = 1.50 + 0.025i$, which is approximately the mean value of measurements by Patterson [1981] between 300–400 nm. For the lognormally distributed long range transport mode of dust with volume median diameter of 2.5 μm [Zender *et al.*, 2003], the single scattering albedo at $\lambda = 300$ nm is 0.64. Previous observations and simulations agree that dust causes significant absorption in the key tropospheric photochemical wavelengths (300–400 nm) [Savoie *et al.*, 2000; Diaz *et al.*, 2001; Kaufman *et al.*, 2001; Dubovik *et al.*, 2002]. The influence of Relative Humidity (RH) on n is neglected since the radiative properties of atmospheric dust are relatively insensitive to RH changes [Li-Jones *et al.*, 1998; He and Carmichael, 1999].

Figure 2 shows the change in photolysis rate coefficients (J values) for $\text{O}(^1\text{D})$ and NO_2 due to scattering and absorption by mineral dust at three dusty locations. Points A (10°N , 15°E) and B (18°N , 5°W) are centers of dust emissions over west Africa in January and July, respectively. Point C (14°N , 32°W) is downwind in the tropical Atlantic. Dust significantly reduces $J_{\text{O}(^1\text{D})}$ and J_{NO_2} in the lower troposphere at all three points. A large seasonal shift is evident in the source regions (cf. Figure 1).

It is interesting to contrast our results at Point A to those of Martin *et al.* [2002], who also employ the Fast-J photolysis code but who use the Ginoux *et al.* [2001] dust distribution. Compared to Martin *et al.*, we predict greater J -rate reductions due to dust in January, but smaller reductions at all altitudes in July. The discrepancy between dust-induced J -rate changes between these models is due to differences between the modeled dust distributions. In DEAD, dust emissions are maximum at Point A in January and then move to the northwest in July, leaving low column dust at Point A (cf. Figure 1).

To place the O_3 response to mineral dust in context, we first show the unperturbed O_3 abundance in Figure 3. This is the O_3 abundance simulated with gas phase chemistry alone. Seasonal biomass burning forms the O_3 maxima in sub-Saharan Africa in January. Industrial emissions of O_3 precursors cause the O_3 maxima in the U.S., Europe, and

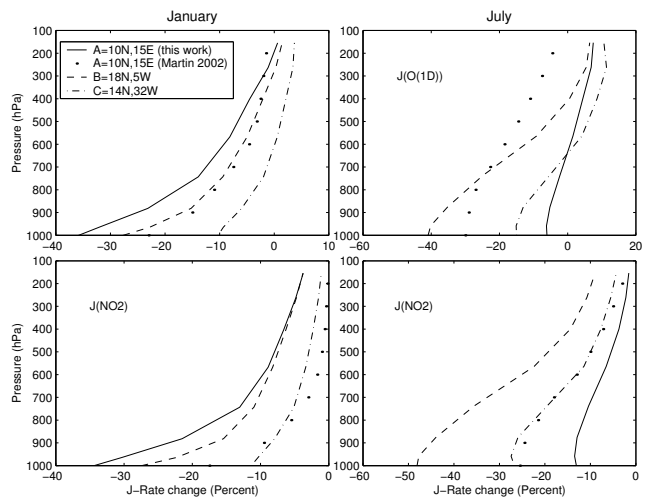


Figure 2. Simulated dust-induced change in J -values. Point A (10°N , 15°E) in this study is solid line, and from simulation of Martin *et al.* [2002] is dotted line. Point B (18°N , 5°W) is dashed line. Point C (14°N , 32°W) is dash-dot line.

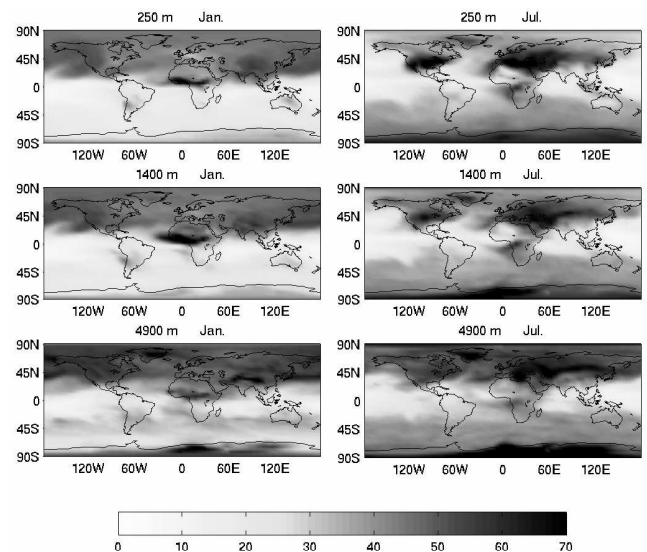


Figure 3. Climatological O_3 [ppb] in January and July at three atmospheric layers simulated using gas phase chemistry alone.

downwind regions in July.

Plate 1 and Figure 4 show the effects of photolysis rate forcing by dust on O_3 and OH, respectively, in January and July. We show only O_3 and OH because they represent the

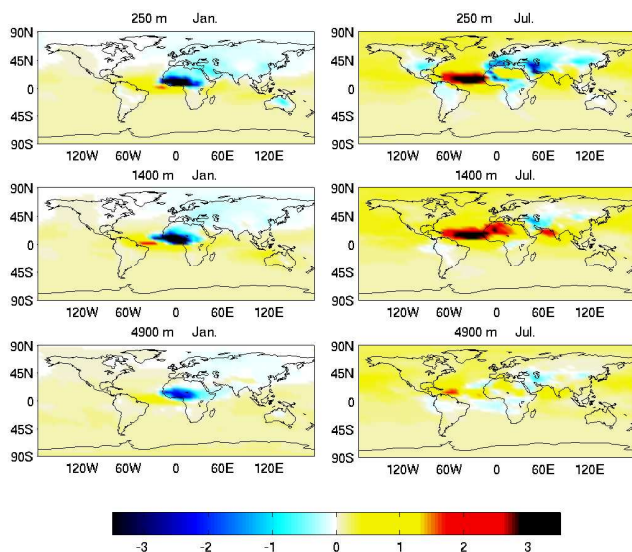


Plate 1. Photolysis rate forcing of O_3 [ppb] by dust in January and July at three atmospheric layers.

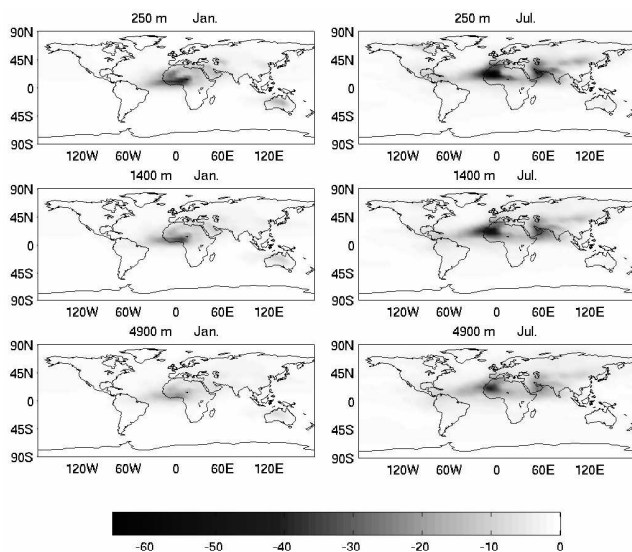


Figure 4. Photolysis perturbation to OH [%] by dust in January and July at three atmospheric layers.

key tropospheric oxidants and drive tropospheric chemistry. The maximum perturbations are in dust source regions in the boundary layer and decrease with altitude. The perturbation patterns are consistent with dust abundance, and show that tropospheric chemistry responds quickly to photochemical forcing. January is characterized by decreased O_3 at all

levels in the African dust region, while a more diffuse O_3 decrease occurs over Asia. In July, there is a striking change in the sign of the O_3 perturbation due to African dust. The Asian dust O_3 perturbation also changes from decreasing to increasing above the boundary layer.

Comparison of Plate 1 and Figure 3 shows that in both January and July the maximum O_3 reduction by dust occurs over continental, high- NO_x , ozone-producing regions. Previous studies show that over low- NO_x oceanic regions, photochemistry destroys O_3 [Olson *et al.*, 1997]. Dust absorption reduces photochemistry, and hence this loss, in low- NO_x oceanic regions. This causes O_3 to increase there [Bian *et al.*, 2003]. The increased O_3 perturbation in remote regions in July is associated with more background dust and higher ozone photochemical production and destruction rate due to the higher solar irradiance and precursor emissions in northern summer.

The tropical Atlantic ocean is an area of particular interest because of its proximity to dust sources. Here the O_3 change is small in January, and increases by more than 3 ppb in July. The nearby upstream dust sources and biomass burning emissions (which provide high- NO_x) are controlling factors in this seasonal change. Biomass burning in the Sahel in January (Figure 3) is close to dust emissions and transport paths in north Africa (Figure 1). However, the centers of dust and biomass burning emissions shift by about 10° in opposite directions in July, separating the dust from the biomass burning plumes. This leaves low- NO_x in the tropical North Atlantic ocean in July. These results are consistent with previous studies which show that absorbing aerosol reduces ground level O_3 in polluted environments [Dickerson *et al.*, 1997; Jacobson, 1998; He and Carmichael, 1999] and that O_3 increases or decreases in the upper atmosphere depending on the availability of NO_x [He and Carmichael, 1999]. The OH decreases in Figure 4 are consistent with the spatial distribution of dust (Figure 1). The decreases are driven by reductions in $O(^1D)$ caused by reduced ultraviolet photolysis of O_3 . The OH decreases are exacerbated by chemical reduction of OH due to reduced NO and increased CO due to photolysis changes [Bian *et al.*, 2003].

Table 1 lists the mean January, July and annual changes in O_3 [%] and OH [%] due to light scattering and absorption by dust. The amplitude of the O_3 perturbation in July in the Northern Hemisphere (NH) is much larger than the Southern Hemisphere (SH) perturbation. This is due to the three factors: absolute dust amount, proximity to O_3 precursors, and relative land area, already mentioned. Interestingly, net photolysis-induced annual mean O_3 changes are greater in the SH than in the NH due to negative O_3 change in the NH winter time. The global annual mean perturbation of O_3 and OH by dust via photolysis is 0.23% and -2.44% , respec-

Table 1. January, July, and Annual mean photochemical perturbation [%] by dust of NH, SH, and Global O₃ and OH.

Region	O ₃			OH		
	Jan	Jul	Ann.	Jan	Jul	Ann.
NH	-0.12	0.98	0.19	-2.51	-4.82	-4.07
SH	0.40	0.21	0.26	-0.68	-1.03	-0.82
Global	0.14	0.59	0.23	-1.59	-2.92	-2.44

tively. The global O₃ perturbation is a factor of four larger in July than in January. The perturbation of both gases is about a factor of four larger in the NH than in the SH in both seasons and in the annual mean (for OH). The annual change in O₃ is about 0.2% in each hemisphere, because the seasonal changes differ dramatically.

3.2. Effects of Heterogeneous Uptake

Direct measurements and theoretical research provide convincing evidence that mineral dust plays important roles in altering atmospheric chemistry through heterogeneous reactions [Goodman *et al.*, 2000; Galy-Lacaus *et al.*, 2002]. Once sequestered on mineral dust particles, oxidants such as HNO₃ and SO₂ appear to undergo fast neutralization reactions with alkaline material (e.g., CaCO₃) in mineral dust [Dentener *et al.*, 1996; Zhang and Carmichael, 1999; Underwood *et al.*, 2001; Michel *et al.*, 2002]. Dentener *et al.* [1996] estimated that at least 40% of total column nitrate is found on the mineral aerosol over vast regions of the NH. We simulate the net direct uptake on mineral dust of O₃, odd-hydrogen (OH, HO₂), odd-nitrogen (NO₂, NO₃, and HNO₃), N₂O₅, and H₂O₂. Heterogeneous reaction of SO₂ on dust is also an important uptake process [Dentener *et al.*, 1996; Song and Carmichael, 2001]. However, we do not include the sulfur cycle in this study. Our results on heterogeneous uptake on dust for some species should be considered an upper bound on dust uptake since some of these species would be lost to heterogeneous reactions on other aerosol types.

Using the method of Schwartz [1986] and Tie *et al.* [2001], the lifetime of species A associated with heterogeneous reactions on particles of radius R_p is provided by the inverse of the pseudo first-order heterogeneous rate constant k for diffusive and kinetic transport of A to the particle surface:

$$k(A, R_p, T) = S[R_p/D_A + 4/(v_A\gamma)]^{-1} \quad (1)$$

Here, v_A is the mean molecular speed of gas species A at temperature T [K]. We will discuss the T -dependence of k

Table 2. Uptake Coefficients of Mineral Dust in UCI CTM

Reaction	Uptake γ	References ^a
H ₂ O ₂ + Dust \rightarrow Products	1.0×10^{-4}	1
HNO ₃ + Dust \rightarrow Products	1.1×10^{-3}	1, 2, 5
HO ₂ + Dust \rightarrow Products	0.1	1, 6
N ₂ O ₅ + Dust \rightarrow Products	1.0×10^{-3}	1, 2
NO ₂ + Dust \rightarrow Products	4.4×10^{-5}	5
NO ₃ + Dust \rightarrow Products	0.1	4, 6
O ₃ + Dust \rightarrow Products	5.0×10^{-5}	1, 2, 6, 3
OH + Dust \rightarrow Products	0.1	6

^aReferences: 1, Dentener *et al.* [1996]; 2, DeMore *et al.* [1997]; 3, Michel *et al.* [2002]; 4, Seinfeld and Pandis [1997]; 5, Underwood *et al.* [2001]; 6, Zhang and Carmichael [1999];

more thoroughly later in this section. D_A is the gas-phase diffusion coefficient of species A in air, and ranges from $1-2 \times 10^{-5} \text{ m}^2 \text{ s}^{-1}$ for most species [Schwartz, 1986; Pruppacher and Klett, 1998]. Measurements of D_A have not been reported for many species modeled here, so we set $D_A = 10^{-5} \text{ m}^2 \text{ s}^{-1}$ for all species as in Tie *et al.* [2001]. S [$\text{m}^2 \text{ m}^{-3}$] is the surface area density of the particles and is determined from the predicted mass mixing ratio of dust in four size bins using the specific area \underline{S} [$\text{m}^2 \text{ kg}^{-1}$] shown in Table 2 of Zender *et al.* [2003]. The mass uptake coefficient of species A is γ .

The uptake coefficients of the eight species considered to undergo irreversible reactions on mineral dust surfaces in our model are summarized in Table 2. Uncertainties in γ are large, up to three orders of magnitude for certain species [Zhang and Carmichael, 1999; Goodman *et al.*, 2000; Michel *et al.*, 2002; Underwood *et al.*, 2001]. For example, recent studies report $2.0 \times 10^{-6} < \gamma < 2.5 \times 10^{-3}$ for O₃ [Michel *et al.*, 2002] and $2.0 \times 10^{-5} < \gamma < 1.6 \times 10^{-2}$ for HNO₃ [Goodman *et al.*, 2000; Underwood *et al.*, 2001]. We apply the values in Table 2 globally so that regional differences in γ due to dust mineralogy and RH are neglected.

Figures 5 and 6 show the reduction of O₃ [ppb] and OH [%], respectively, due to heterogeneous reactions on dust. Since the net uptake is irreversible, mineral dust uptake reduces O₃ and OH globally. Heterogeneous uptake of O₃ by dust (Figure 5) is broadly controlled by two factors: the O₃ abundance (Figure 3) and the horizontal and vertical distributions of dust (Figure 1). In January, the maximum reduction occurs along the plume from western Africa to the tropical Atlantic ocean just above the boundary layer. In

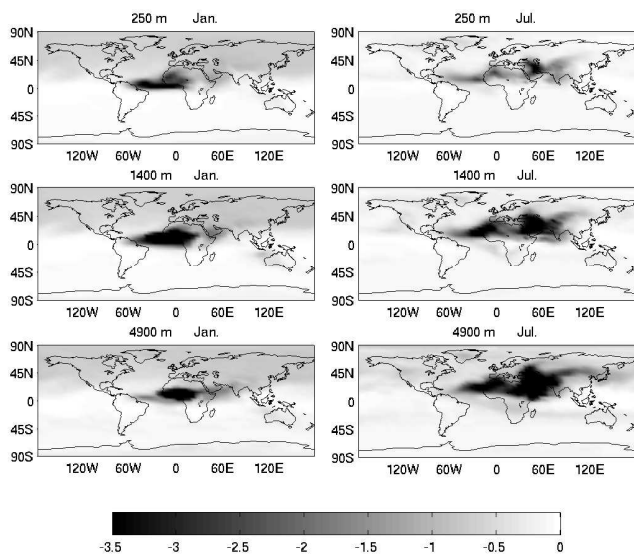


Figure 5. Decrease in O_3 [ppb] due to heterogeneous reactions on dust in January and July at three atmospheric layers.

our simulations African dust that is lifted above the boundary layer in January is conveyed over the Atlantic ocean in a layer between 1–3 km known as the Saharan Air Layer (SAL) [Karyampudi et al., 1999]. The O_3 change is greatest near the top of the boundary layer where the local maxima in O_3 abundance (Figure 3) coincides with the SAL.

In July, O_3 uptake over Asia becomes significant and increases with altitude. This is due to meteorology and O_3 and dust concentrations. The Arabian peninsula has less dust, but much more O_3 , than west Africa in July. Asian O_3 abundance is elevated by pollution transport from Europe and by stratospheric intrusions near Tibet, but west African O_3 has decreased as biomass burning shifts south of the equator. Thus heterogeneous forcing by dust causes stronger O_3 depletion in Asia than in west Africa, especially in the mid-troposphere. High O_3 abundance over the Arabian desert and strong vertical transport of dust are the factors driving the stronger uptake in Asia. The summertime Tibetan low pressure cell facilitates convective transport and displaces the region of heterogeneous uptake to higher altitudes. It is interesting that the O_3 response to heterogeneous uptake increases with altitude in July, especially over Asia, while the photochemical response of O_3 to dust decreases with altitude (Plate 1).

Figure 6 shows that heterogeneous chemistry is important for OH over the dusty regions in both January and July. This is consistent with the OH photolytic perturbation (Figure 4). OH uptake favors lower altitudes than O_3 uptake (Figure 5).

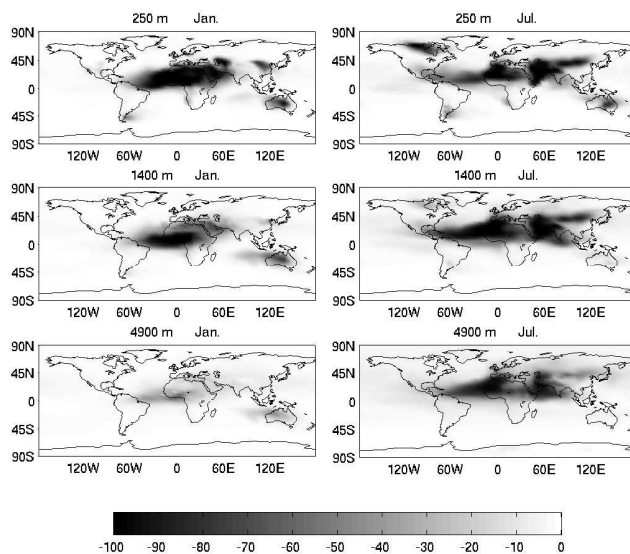


Figure 6. Decrease in OH [%] due to heterogeneous reactions on dust in January and July at three atmospheric layers.

Table 3. January, July, and Annual mean decrease [%] in NH, SH, and Global O_3 and OH due to heterogeneous reactions on dust.

Region	O_3			OH		
	Jan	Jul	Ann.	Jan	Jul	Ann.
NH	-1.52	-1.43	-1.48	-10.97	-19.96	-16.35
SH	-0.46	-0.33	-0.30	-3.67	-3.11	-2.86
Global	-0.99	-0.88	-0.89	-7.32	-11.54	-9.60

This reflects the quicker response of OH to indirect effects. The gas phase lifetime is only seconds for OH but often exceeds a few days for O_3 .

Table 3 lists the mean January, July, and annual changes in O_3 [%] and OH [%] due to heterogeneous chemistry on dust. Globally, O_3 decreases 0.9% and OH decreases nearly 10%. Regional reductions reach 8.5% for O_3 at the top of boundary layer over west Africa and the tropical Atlantic Ocean in January and in the mid-troposphere over the Arabian desert in July. OH decreases by $\sim 80\%$ within the boundary layer in the zonally extensive tropical region from northern Africa to the Atlantic ocean in January and by $\sim 50\%$ from India to the Caribbean in July. Our interpolated monthly mean dust fields contribute to excessive OH uptake in very dusty regions by not allowing dust-free periods during which OH could temporarily recover. The larger chemical perturbation occurs in the NH, where trace gas re-

ductions are more than triple those in the SH. Heterogeneous uptake changes global O_3 and OH about four times more than photolysis rate forcing. This result is not quantitatively robust since our predicted changes in OH are large, as is the uncertainty in the uptake coefficients (Table 2). We are quantifying these uncertainties in a separate study.

Unfortunately, field measurements which could confirm or deny our findings for climatological heterogeneous uptake of oxidant species on mineral surfaces in dusty regions are scarce [Bey *et al.*, 2001]. Previous research has focused on the heterogeneous perturbation in dusty conditions. Using a global three-dimensional model, Dentener *et al.* [1996] estimated that heterogeneous uptake on dust leads to a $\sim 10\%$ reduction of O_3 in dust source regions during the dustiest season. Using a box model, Zhang and Carmichael [1999] estimated that spring dust storms in East Asia decrease O_3 by 11–40%, NO_y ($NO_3+N_2O_5+HNO_3$) by 16–100%, and H_xO_y ($OH+HO_2+H_2O_2$) by 11–59% via heterogeneous uptake. Our simulations indicate global reductions due to heterogeneous uptake on dust of 0.9% for O_3 , 3.9% for NO_y , and 5.1% for H_xO_y . Thus our global estimates are an order of magnitude less than estimates from other models during dusty conditions. In dusty parts of North Africa during late winter and early spring, we predict boundary layer ozone reductions of $\sim 10\%$, similar to Dentener *et al.* [1996]. In East Asia in spring, we predict the monthly mean O_3 decreases by about 2%. This is consistent with the 11–40% instantaneous O_3 reduction during spring dust events in East Asia reported by Zhang and Carmichael [1999]. (Dust concentrations during these events are an order of magnitude larger than the monthly mean concentrations.)

3.3. Photochemical and Heterogeneous Coupling

Sections 3.1–3.2 describe the photolytic and heterogeneous forcing of oxidants by dust, examining each process in isolation. We now quantify interactions between photolytic and heterogeneous forcing when those processes operate simultaneously, as in nature. We define the effects of the photolysis-rate-only, heterogeneous-only, and coupled (photolysis plus heterogeneous) forcing by dust as Δ_P , Δ_H , and Δ_{P+H} respectively. The degree of non-linear interaction between photolysis and heterogeneous effects of dust defines the coupling factor λ

$$\lambda = \Delta_{P+H}/(\Delta_P + \Delta_H) \quad (2)$$

Values of λ near unity indicate that the individual Δ_P and Δ_H perturbations are additive (i.e., linear). Plate 2 shows the zonal mean λ_{O_3} , λ_{OH} , and λ_{HNO_3} in January and July. In most remote and upper tropospheric regions, λ is near unity. In these regions, feedbacks between the photolytic and heterogeneous perturbations are generally less than 10%. The

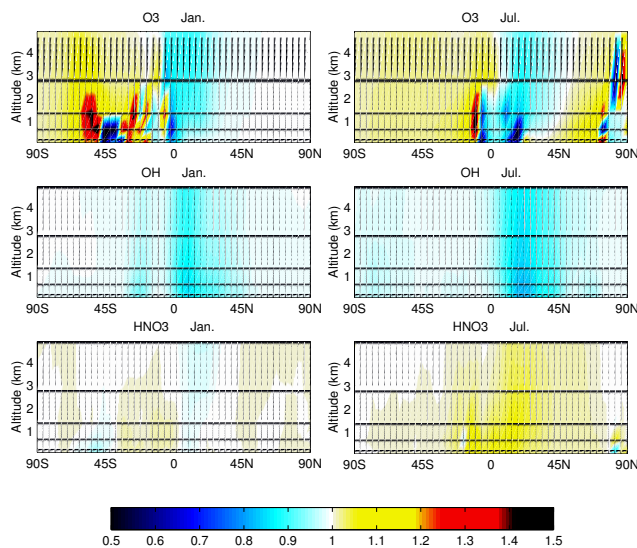


Plate 2. Zonal mean coupling factor λ between photolysis rate and heterogeneous dust forcing of O_3 , OH, and HNO_3 in January (left column) and July (right).

interaction increases over the subtropics, especially in the NH, where most dust resides. Feedbacks of O_3 production and loss due to changes in O_3 precursors leads to the complicated structure of λ_{O_3} . Involvement of O_3 in photolysis alteration is negligible in its contribution to λ_{O_3} magnitude and structure. Coupling amplifies O_3 reductions in most of the SH and suppresses it in the tropics and NH in January. The effect of coupling in July is similar except in the NH mid-to-high latitudes where coupling changes from a suppressing to an amplifying effect on O_3 . Strong coupling occurs in the boundary layer and lower troposphere from the equator to $50^\circ S$ in January and in the NH subtropical boundary layer and high latitudes in July. Other species studied in this paper exhibit coupling patterns similar to OH or to HNO_3 .

We now examine the relative roles of Δ_P and Δ_H in determining Δ_{P+H} , and how the vertical structure of dust affects this relationship. We define the relative contribution of photolysis, δ_P , to Δ_{P+H} , the net species change by dust, as

$$\delta_P = \frac{\Delta_P}{|\Delta_P| + |\Delta_H|} \quad (3)$$

Thus $0 < |\delta_P| < 1$ and $|\delta_P| = 0.5$ where the magnitudes of the photolysis-only effect and the heterogeneous-only effect of dust are equal. Strictly, this definition is only valid where $\lambda = 1$. We take this definition approximately due to the weak nonlinear interaction on global scale (Plate 2). The relative contribution of heterogeneous reactions, δ_H (not

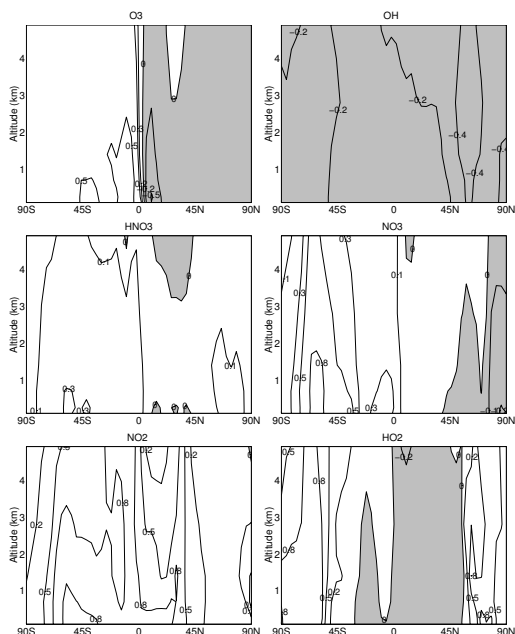


Figure 7. Relative role of photolysis δ_P in altering six species in Table 2 in January. Shading indicates $\delta_P < 0$.

shown) is defined analogously to (3). Heterogeneous uptake is negative definite, so that $\delta_H \equiv -1 + |\delta_P|$. Thus $|\delta_P|$ is small where $|\delta_H|$ is large, and visa versa.

Figures 7 and 8 show the zonal mean δ_P for six of the species in Table 2 in January and July, respectively.

Most regions dominated by photolysis perturbation (i.e., $|\delta_P| > 0.5$) are confined to low-to-mid altitudes. This is consistent with our results in the previous section that heterogeneous forcing by dust is almost four times larger than the photolysis rate forcing. Patterns of δ_P for O_3 and odd-nitrogen are similar. All show large values in the SH mid-latitude boundary layer in January and in tropics and the NH high latitudes in July. Among these species, NO_2 is most changed by photolysis, with extensive vertical and meridional regions of large $|\delta_P|$. Odd-hydrogen (OH and HO_2) shows large $|\Delta_P|$ in polar regions in both seasons.

Table 4 summarizes the annual mean changes due to photolysis-only Δ_P , heterogeneous-only Δ_H , and the coupled forcing of dust, Δ_{P+H} . The NH change dominates the SH change for most species, in accord with the hemispheric asymmetry of dust mass. Global annual mean tropospheric O_3 , H_2O_2 , NO_2 , and N_2O_5 change less than or around 1%; HNO_3 , HO_2 , and NO_3 change 3–6%, and OH changes by –11.1%. OH and HO_2 are the most sensitive species in our study because photolysis rate and heterogeneous forcing by

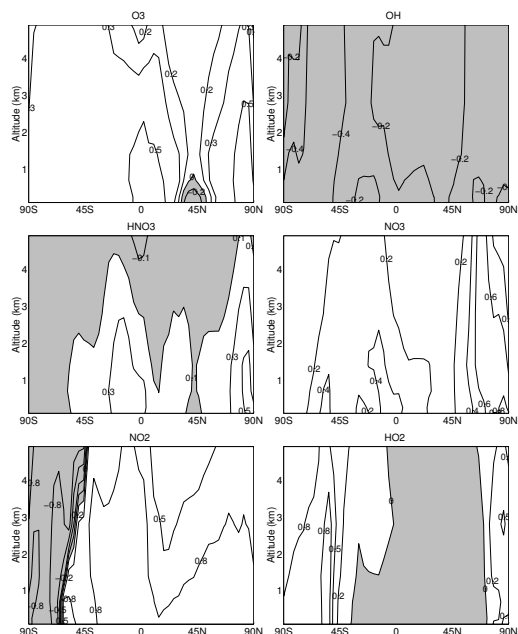


Figure 8. Same as Figure 7 except for July.

dust both decrease their abundance. In contrast, the individual changes Δ_P and Δ_H are of opposite signs for O_3 , odd-nitrogen, N_2O_5 , and H_2O_2 . Thus cancellation by opposing responses to dust results in smaller net changes Δ_{P+H} for these species.

Table 4 also lists the global mean coupling factors λ (2). In the global mean, OH is the most sensitive to coupling—7% of its change is due to the interaction of the photochemical and heterogeneous responses to dust forcing. O_3 exhibits no sensitivity to coupling ($\lambda_{O_3} = 1$) in the global mean due to mutual cancellation of regions of positive and negative coupling (Plate 2). On regional scales, however, O_3 exhibits moderate coupling.

We demonstrate this by examining the effects of dust on atmospheric chemistry in a dust-dominated region. This is Northern Africa and Tropical Atlantic (NATA) region downwind (80W–30E, 0–30N). This NATA region carries the largest dust burden on the planet due to African dust sources [e.g., Zender *et al.*, 2003]. Figure 9 shows the seasonal cycles of the dust forcing (Δ_P , Δ_H , and Δ_{P+H}) of each species in Table 2. The photolysis rate forcings peak in spring for OH, HNO_3 , and HO_2 , and in summer for O_3 , NO_3 , NO_2 , N_2O_5 . This seasonal change is also consistent with regional seasonality of dust burden from observations [Savoie *et al.*, 1992; Holben *et al.*, 1998] and simulations [Ginoux *et al.*, 2001; Zender *et al.*, 2003]. The net dust forcing of atmospheric chemistry is substantially larger in this region (see Ta-

Table 4. Annual mean changes [%] of eight species due to effects of dust. Shown are Δ_P , Δ_H , and Δ_{P+H} in NH, SH, Global mean, and North Africa and the Tropical Atlantic (NATA) region downwind (80W–30E, 0–30N), and global mean and NATA-region coupling factors λ (2).

	Photolysis Δ_P				Heterogeneous Δ_H				Coupled Δ_{P+H}				λ	
	NH	SH	Global	NATA	NH	SH	Global	NATA	NH	SH	Global	NATA	Global	NATA
O ₃	0.2	0.3	0.2	0.9	-1.5	-0.3	-0.9	-5.0	-1.3	-0.0	-0.7	-3.8	1.00	0.93
OH	-4.0	-0.8	-2.4	-15.0	-16.4	-2.9	-9.6	-64.0	-18.5	-3.6	-11.1	-66.8	0.93	0.85
HNO ₃	0.4	0.3	0.3	0.8	-6.1	-1.5	-3.8	-28.3	-5.8	-1.2	-3.5	-27.7	1.00	1.01
HO ₂	-1.0	0.2	-0.4	-6.0	-9.1	-1.1	-5.1	-43.5	-9.6	-0.9	-5.2	-45.3	0.95	0.92
NO ₂	1.9	0.8	1.3	5.4	-10.2	-1.5	-5.9	-47.2	-8.7	-0.8	-4.7	-44.2	1.02	1.06
NO ₃	2.1	0.7	1.4	9.8	-0.5	-0.2	-0.3	-6.9	1.6	0.5	1.1	3.1	1.00	1.07
N ₂ O ₅	3.3	1.2	2.2	12.0	-3.4	-0.8	-2.1	-19.6	-0.3	+0.4	0.0	-9.4	—	1.24
H ₂ O ₂	0.3	0.7	0.5	-0.6	-0.4	0.1	-0.2	-2.2	-0.2	0.8	0.3	-3.0	1.00	1.07

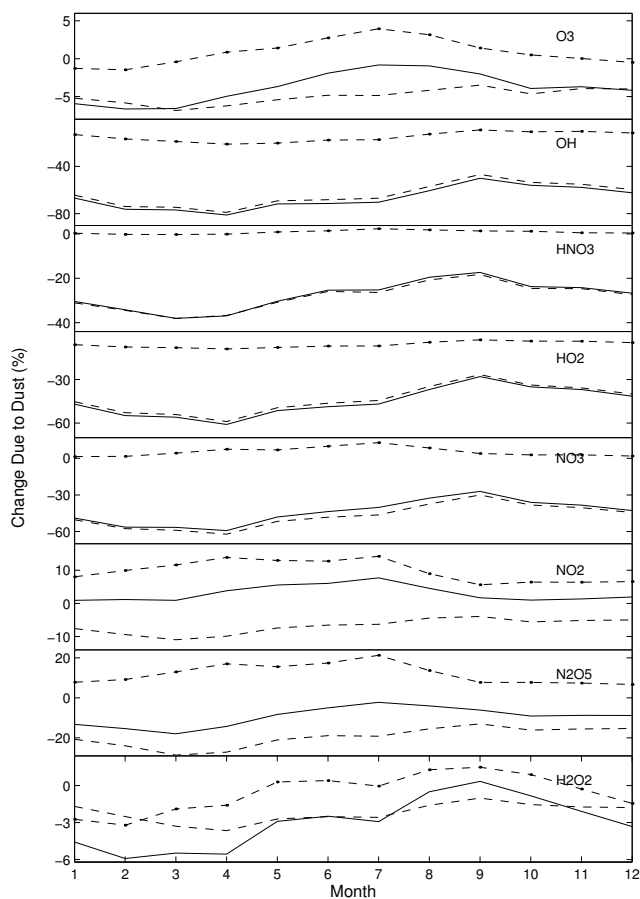


Figure 9. Seasonal cycle of chemical changes in north Africa and tropical Atlantic region downwind (80W–30E, 0–30N). Shown are photolysis-only Δ_P (dot-dash), heterogeneous-only Δ_H (dash), and coupled Δ_{P+H} (solid) forcings of dust.

ble 4) than in the global mean. For instance, OH reduction in this region reaches -66.8% , six times the global mean OH change. Table 4 shows that the influence of photolysis-heterogeneous coupling is much stronger in the NATA re-

gion than in the global mean. Coupling accounts for 7%, 15%, and 24% of the change of O₃, OH, and N₂O₅, respectively, in the NATA region.

Our results are consistent with previous regional studies of dust-chemistry interactions in Asia. Zhang *et al.* [1994] observed short term anti-correlations of O₃ and dust concentrations in Haplo, Japan. They estimated O₃ decreases about 3–10% per 10 $\mu\text{g m}^{-3}$ dust. Our simulated annual mean boundary layer dust concentration in Haplo, Japan is about 1.2 $\mu\text{g m}^{-3}$ [Zender *et al.*, 2003]. We estimate $\Delta_{P+H}O_3$ is about -1.2% in fall, -1.3% in winter, and -1.5% in spring (consistent with Zhang *et al.*), and $+0.4\%$ in summer.

Figure 10 compares our modeled O₃ profile to observations at Abidjan (5°N, 4°W) made during the MOZAIC aircraft program from 1994–1999 [Martin *et al.*, 2002]. The January simulation improves in the lower troposphere when we account for the effects of mineral dust on chemistry. The simulated influence of dust on the O₃ profile in July is not obvious due to the cancellation of positive photolysis forcing and negative heterogeneous forcing over this station.

Tabazadeh *et al.* [1998] propose heterogeneous chemistry on mineral dust and biomass burning aerosols irreversibly removes gaseous HNO₃. If so, then representing this process should help reduce high biases in HNO₃ common to gas-phase-only models. For example, previous studies of the nitrogen cycle simulated summertime HNO₃ levels 2–10 times larger than observed in the upper troposphere over the east China coast [Hauglustaine *et al.*, 1998; Wang *et al.*, 1998b]. The UCI CTM summertime HNO₃ bias in this region is also close to a factor of two. We find that dust reduces HNO₃ by about 60% in the mid-to-upper troposphere in and downwind of dust source regions in summer, and by about 40% in winter. Based on our best estimate uptake rates (Table 2), therefore, dust explains a significant portion of HNO₃ biases as proposed by Tabazadeh *et al.* [1998]. Remaining model-observation differences could be further, but probably not completely, reconciled if we are underestimating uptake rates and/or dust surface area in this region. Dust and NO_x are often in the same plume and it is possible that in-

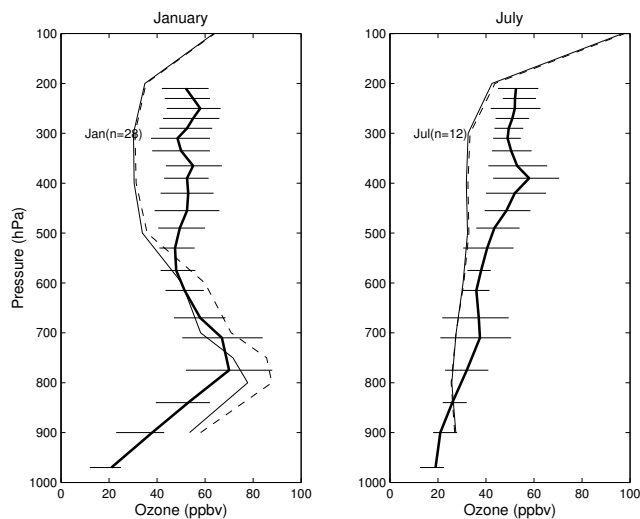


Figure 10. Ozone model-observation comparison over Abidjan (5°N , 4°W) in January and July. 1994–1999-mean MOZAIC measurements [Martin et al., 2002] are thick solid lines. Error bars indicate standard deviations. Number of observations for each month is in parentheses. Model results are shown with (thin solid lines) and without (dashed lines) mineral dust.

terpolated monthly mean dust used here underestimates the impact of dust on HNO_3 . Further investigation is needed to quantify these uncertainties.

3.4. Sensitivity to Dust Spatial Distribution

In this section we examine the sensitivity of column ozone change to dust horizontal, vertical, and geographic distribution. Our goal here is to link the efficiency with which dust alters important oxidants like O_3 to physical processes, so that we understand where and why oxidants are most sensitive to marginal changes in dust emissions. We define the net O_3 forcing efficiency of dust $\epsilon_{\text{P}+\text{H}}$ as the change in tropospheric column O_3 [%] normalized by the column mass of dust in mg m^{-2} . The analogous forcing efficiencies due to photolysis-only and heterogeneous-only forcing are ϵ_{P} and ϵ_{H} .

Figure 11a shows the zonal mean column dust burden [mg m^{-2}] in July. The vertical scale is logarithmic and shows the dramatic variation of dust with latitude. Figure 11b shows the July change in tropospheric O_3 [%] due to the photolysis-only and the heterogeneous-only effects of dust. Figure 11c shows the forcing efficiencies ϵ_{P} and ϵ_{H} (i.e., the ratio of panel b to panel a). Note the scale is logarithmic. Both ϵ_{P} and ϵ_{H} increase toward high latitudes, be-

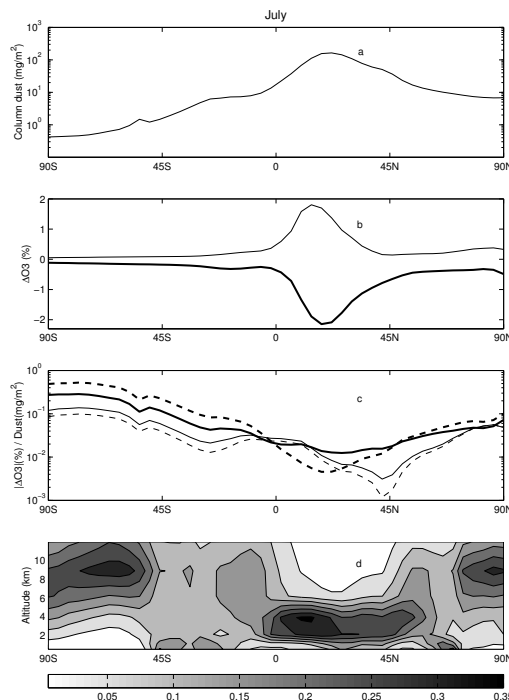


Figure 11. July zonal mean (a) column dust burden [mg m^{-2}], (b) tropospheric O_3 change [%] due to normal dust distribution broken down into Δ_{P} (thin line) and Δ_{H} (thick line), (c) O_3 forcing efficiencies of dust by photolysis forcing ϵ_{P} (thin line) and heterogeneous uptake ϵ_{H} (thick line). Dashed lines show corresponding $\tilde{\epsilon}_{\text{P}}$ and $\tilde{\epsilon}_{\text{H}}$ for the inverted dust distribution. (d) Normalized vertical distribution of dust.

coming several times larger in polar regions than in the NH subtropics. Thus O_3 change is far greater in remote regions, per unit local column dust mass, than in source regions. At first glance it appears that a small amount of dust transported to polar regions causes an inordinate change in polar O_3 . However, this depends on whether O_3 change at high latitudes is due to local dust or to the advection of perturbed O_3 from dustier regions.

In July, total dust burden decreases monotonically away from the NH subtropical source region (Figure 11a). The O_3 forcing peaks in the NH subtropics with slight variations in the other latitudes (Figure 11b). To determine the relative importance of transport and local chemistry in the polar regions, we diagnosed separately the advective and local chemical contributions to the O_3 budget in the region 72° – 90°N . In our gas-phase-only simulation, horizontal advection is an order of magnitude more important than the local chemistry in determining O_3 . With dust, the change of O_3

in this region due to horizontal advection is about five times more than the change from local chemistry. Thus O_3 change in non-dusty Northern high latitudes is controlled by transport of perturbed O_3 from the NH midlatitudes and subtropics. Consequently, O_3 change at high latitudes appears to be insensitive to model biases in high latitude dust.

The strong meridional gradient in ϵ_P is also a function of the meridional gradient in the vertical structure of dust. Figure 11d shows the normalized vertical structure of dust. This is obtained by dividing the dust column by the local mass (so the values in each column sum to unity). Dust in source regions is concentrated in the lower troposphere in July (cf. Figure 1b). At the same time, dust reaching the remote high latitudes is concentrated in the upper troposphere where scavenging processes for these clay-sized ($D < 2.5 \mu\text{m}$) particles are inefficient [Zender *et al.*, 2003]. Thus the vertical structure of dust is inverted during transport from source regions to high latitudes.

We studied the sensitivity of ozone forcing to the vertical distribution of dust by inverting the vertical profile of the dust while fixing the total dust column amount. In this sensitivity study, therefore, high-latitude dust is concentrated near the surface, while NH subtropical dust is concentrated in the upper troposphere. Figure 11c shows both the photolysis and heterogeneous forcing efficiencies derived from the realistic dust vertical distribution, ϵ_P and ϵ_H , and the efficiencies of the inverted dust distribution, $\tilde{\epsilon}_P$ and $\tilde{\epsilon}_H$. The significant separation between ϵ_P and $\tilde{\epsilon}_P$ (the scale is logarithmic), as well as between ϵ_H and $\tilde{\epsilon}_H$, shows the strong vertical sensitivity of the O_3 forcing efficiency.

Dust high in the atmosphere alters column O_3 through photolysis more than the same amount of dust in the lower atmosphere. However, $\tilde{\epsilon}_P < \epsilon_P$ in the NH subtropics. As discussed in Section 3.1, dust in low- NO_x environments increases O_3 by reducing photochemical destruction of O_3 . In the normal dust vertical distribution, lower tropospheric dust from northern Africa lies beneath the mid-to-upper tropospheric NO_x from southern African biomass burning regions, resulting in increased O_3 in the dusty region. In the inverted dust scenario, upper tropospheric dust mixed with high- NO_x reduces photolytic O_3 there.

The largest discrepancy between ϵ_P and $\tilde{\epsilon}_P$ occurs near 45°N . Dust near 45°N that normally resides between 2–4 km is located between 5–8 km in the inverted experiment. European emissions of O_3 precursors in NH summer create a strong O_3 band in the Eurasian mid-latitudes near 5 km (Figure 3). In the inverted dust experiment, dust in the high- NO_x Eurasian mid-troposphere causes substantial O_3 reductions there. The negative O_3 change over land cancels the positive O_3 change over ocean resulting in a small zonal mean $\tilde{\epsilon}_H$ near 45°N . The difference between ϵ_P and $\tilde{\epsilon}_P$ gen-

erally keeps constant or weakens toward the poles. Thus O_3 change in remote regions is more sensitive to global O_3 transport than to dust vertical structure.

The difference between ϵ_H and $\tilde{\epsilon}_H$ tracks the normalized dust distribution in Figure 11d. Where dust normally resides in the lower troposphere, $\epsilon_H > \tilde{\epsilon}_H$, and visa versa. In the troposphere, inverting the dust has little effect on the amount of O_3 the dust is exposed to because the zonal mean vertical distribution of O_3 is relatively homogeneous. Thus the discrepancy between ϵ_H and $\tilde{\epsilon}_H$ is largely explained by the increase of heterogeneous uptake with temperature, $v_A \propto \sqrt{T}$ in (1).

In a box model study, *He and Carmichael* [1999] reported that surface O_3 decreases slightly by dust photochemical forcing when the aerosol layer is raised within the boundary layer, but that O_3 stops changing as the aerosol layer is raised further. Our results indicate that in the real atmosphere the sensitivity of O_3 to the vertical location of dust is more complicated than this and can change signs depending on the presence of O_3 precursors. We find that in dusty regions, O_3 is sensitive not only to the height of the dust layer, but also to NO_x availability. In remote regions O_3 transport is more important than local dust vertical structure.

4. Conclusions

We simulated and analyzed the influence of mineral dust on tropospheric chemistry through its impact on atmospheric photolysis and heterogeneous chemistry. The global annual mean change due to dust is on the order of several percent for most species considered, except for OH (–11.1%) (Table 4). As expected the largest changes occurred in and downwind of dust source regions, e.g., northern Africa, the tropical Atlantic, and the Arabian peninsula (Plate 1, Figures 4, 5, and 6). Changes in O_3 and OH due to dust are more than five times greater in the NH than in the SH (Table 4).

To examine the coupling between photolysis rate forcing and heterogeneous forcing, we defined a coupling factor λ (2) as the ratio of the forcing by both processes acting simultaneously to the sum of the forcings of each process acting alone (Section 3.3). Photolysis forcing and heterogeneous forcing by dust are weakly coupled in the global mean, and moderately coupled over dusty regions. In northern Africa and the tropical Atlantic downwind, coupling accounts for 24%, 15%, and 7% of the changes in N_2O_5 , OH, and O_3 , respectively (Table 4). Studies which neglect photolysis-heterogeneous coupling in dusty regions are likely to have biases of these magnitudes. Globally, heterogeneous uptake weakly modifies the atmospheric photolysis field by reducing tropospheric O_3 , but this indirect effect has no significant impact on photolysis rates. Photolysis forcing generally

produces more O_3 , but uptake of this additional O_3 is also a second-order effect.

Dust horizontal and vertical distributions influence column ozone in subtle ways. High latitude O_3 change is dominated by transport of O_3 altered by dust close to source regions. Therefore, uncertainties in dust concentration near the poles do not propagate to O_3 changes. In dusty regions, the photolysis forcing efficiency of O_3 by dust is not only sensitive to the vertical structure of dust, but also to the coincidence of O_3 precursors. In remote regions O_3 photolysis forcing is not sensitive to dust vertical structure. The heterogeneous uptake efficiency of O_3 by dust is sensitive to the vertical structure of dust, mainly through the influence of temperature on uptake rates.

There are many uncertainties in our results. First, DEAD predicts lower global emission, burden, and optical depth of dust than some other recent estimates [Ginoux *et al.*, 2001; Zender *et al.*, 2003]. Thus, our present results are based on a conservative estimate of dust abundance. Second, like many recent studies [e.g., Lohmann *et al.*, 1999; Ginoux *et al.*, 2001; Woodward, 2001; Martin *et al.*, 2002; Colarco *et al.*, 2003b], we restrict our attention to dust of size $0.1 \lesssim D \lesssim 10 \mu\text{m}$. This is reasonable since Zhang and Carmichael [1999] show that most nitrate and sulfate is found on dust particles with $1.5 < D < 10 \mu\text{m}$. However, models appear to under-estimate the mass fraction of $D > 3 \mu\text{m}$ dust relative to observations in and downwind of dust source regions [Li-Jones and Prospero, 1998; Reid *et al.*, 2003]. Since a given mass of large particles exerts less photolysis rate and heterogeneous forcing than the same mass of smaller particles. Our estimates of dust optical depth are reasonable [Zender *et al.*, 2003; Luo *et al.*, 2003], so our underestimate large dust particles may not induce large errors. Furthermore, large particles have short atmospheric lifetimes so climatological errors in our study will be small.

At least two studies report that indirect forcing by sulfate aerosol decreases by 20% when the aerosol is simulated interactively rather than interpolated from monthly means [Feyl *et al.*, 1997; Rotstajn and Lohmann, 2003]. The sulfate indirect effect depends strongly on non-linear relationships between aerosols, clouds, and radiative fluxes. Mineral dust is not as efficient a CCN as sulfate, therefore the non-linear relation between dust and clouds may be weaker than that of sulfate. However, dust and NO_x are often in the same plume, e.g., in east Asia in spring and in west Africa in northern winter. Our model predicts NO_x dynamically with a full chemistry scheme, but uses interpolated monthly mean dust abundances. This artificially suppresses dust concentration during dust events and promotes the concentration between events. We showed that the presence O_3 precursors like NO_x significantly affects the chemical forcing by

dust. Thus non-linear relationships between dust, O_3 precursors, and their chemical responses may be biased in our model simulations. Further investigation is needed to quantify these potential biases.

The uncertainty in our estimates of the photochemical forcing of mineral dust stems from the choice of refractive index n compounded by regional biases in the size and vertical distribution [Bian *et al.*, 2003]. Previous studies show that dust strongly absorbs in the near ultraviolet, and that n varies with wavelength [Savoie *et al.*, 2000; Diaz *et al.*, 2001; Kaufman *et al.*, 2001; Dubovik *et al.*, 2002]. Although the constant dust refractive index adopted in this study (Section 3.1) results in strong absorption at key tropospheric photochemical wavelengths (300–400 nm), it should have a strong wavelength dependence.

The uptake coefficients in Table 2 are taken to be globally uniform, although the mineralogical composition of dust varies with sources [Sokolik *et al.*, 2001; Michel *et al.*, 2002]. We emphasize that our results are sensitive to our choice of uptake coefficient values which have large uncertainties. An analysis of the sensitivity our results to these uncertainties in γ is underway and we hope it will help prioritize future laboratory research on γ . Gaseous uptake may also vary with Relative Humidity through two mechanisms. First, high RH may significantly increase the surface area on deliquescent particles [Hänel, 1976]. Second, RH may increase γ for some gases, such as HNO_3 , but not others, such as NO_2 [Underwood *et al.*, 2001]. Unfortunately, $\gamma(\text{RH})$ for most interesting species is unknown. The resulting biases may be small since RH is low in arid source regions, and particle surface area is low in most ocean regions except the tropical North Atlantic.

Due to these uncertainties in model inputs, this study should be regarded as exploratory and subject to further improvements, including improved model evaluation. Unfortunately, field data to evaluate modeled dust photochemical and heterogeneous effects are limited. Few comprehensive measurements of O_3 have been performed in dusty regions, and the available observations, being for limited field experiments, do not provide representative climatologies. Records for other photochemically active species are also sparse. Recent field campaigns such as ACE-Asia and ITCT 2k2 will greatly facilitate future studies since these campaigns were conducted in and downwind of dust source region during Asian dust outbreaks. Fully evaluating the seasonality, geographic location, and vertical structure of dust perturbation predicted by our model, however, will require sustained measurements in dusty regions.

Acknowledgments. We thank V. Grassian for providing data on uptake rates and M. Prather for helpful comments. We are grate-

ful to P. Jöeckel for providing code to re-grid netCDF data. Helpful comments from two anonymous reviewers substantially improved the quality of the final paper. This research was supported by NASA Grants NAG5-10147 and NAG5-10546.

References

- Atkinson, R., D. Baluch, R. Cox, R. Hampson, J. Kerr, and M. Troe, Evaluated kinetic, photochemical and heterogeneous data for atmospheric chemistry: Supplement V — IUPAC Subcommittee on Gas Kinetic Data Evaluation for Atmospheric Chemistry, *J. Phys. Chem. Ref. Data*, *26*, 521–1011, 1997. 2.1
- Balis, D. S., C. S. Zerefos, K. Kourtidis, A. F. Bais, A. Hofzumahaus, A. Kraus, R. Schmitt, M. Blumthaler, and G. P. Gobbi, Measurements and modeling of photolysis rates during the PAUR II campaign, *Submitted to J. Geophys. Res.*, 2001. 1
- Baughcum, S. L., T. G. Tritz, S. C. Henderson, and D. C. Pickett, Scheduled civil aircraft emission inventories for 1992: Database development and analysis, *Tech. Rep. Tech. rept. NASA CR-4700*, National Aeronautics and Space Administration, Langley Research Center, Hampton, VA, 1996. 2.1
- Bey, I., D. J. Jacob, J. A. Logan, and R. M. Yantosca, Asian chemical outflow to the pacific in spring: Origins, pathways, and budgets, *J. Geophys. Res.*, *106*, 23097–23113, 2001. 3.2
- Bian, H., Improvement and application of UCI chemistry transport model, Ph.D. thesis, Department of Earth System Science, University of California, Irvine, 2001. 2.1
- Bian, H., and M. J. Prather, Fast-J2: Accurate simulation of stratospheric photolysis in global chemistry models, *J. Atmos. Chem.*, *41*, 281–296, 2002. 2.1, 3.1
- Bian, H., M. Prather, and T. Takemura, Tropospheric aerosol impacts on trace-gas budgets through photolysis, *J. Geophys. Res.*, *108*, 4242, doi:10.1029/2002JD002743, 2003. 1, 3.1, 3.1, 4
- Carver, G. D., P. D. Brown, and O. Wild, The ASAD atmospheric chemistry integration package and chemical reaction database, *Comput. Phys. Commun.*, *105*, 197–215, 1997. 2.1
- Colarco, P., O. Toon, and B. Holben, Saharan dust transport to the caribbean during PRIDE: Part 1. Influence of dust sources and removal mechanisms on the timing and magnitude of downwind AOD events from simulations of and remote sensing observations, *J. Geophys. Res.*, *108*, 8589, doi:10.1029/2002JD002658, 2003a. 2.2
- Colarco, P., et al., Saharan dust transport to the caribbean during PRIDE: Part 2. Transport, vertical profiles, and deposition in simulations of in situ and remote sensing observations, *Submitted to J. Geophys. Res.*, 2003b. 4
- Collins, W. D., P. J. Rasch, B. E. Eaton, B. Khattatov, J.-F. Lamarque, and C. S. Zender, Forecasting aerosols using a chemical transport model with assimilation of satellite aerosol retrievals: Methodology for INDOEX, *J. Geophys. Res.*, *106*, 7313–7336, 2001. 2.2
- Collins, W. D., P. J. Rasch, B. E. Eaton, D. W. Fillmore, J. T. Kiehl, C. T. Beck, and C. S. Zender, Simulation of aerosol distributions and radiative forcing for INDOEX: Regional climate impacts, *J. Geophys. Res.*, *107*, 8028, doi:10.1029/2000JD000032, 2002. 2.2
- DeMore, W. B., S. P. Sander, D. M. Golden, R. F. Hampson, M. J. Kurylo, C. J. Howard, A. R. Ravishankara, C. E. Kolb, and M. J. Molina, Chemical kinetics and photochemical data for use in stratospheric modeling, *Evaluation Number 12 97-4*, Jet Propulsion Laboratory, Pasadena Calif., 1997. 2.1, 2
- Dentener, F. J., G. R. Carmichael, Y. Zhang, J. Lelieveld, and P. J. Crutzen, Role of mineral aerosol as a reactive surface in the global troposphere, *J. Geophys. Res.*, *101*, 22869–22889, 1996. 1, 3.2, 1, 3.2
- Diaz, J. P., F. J. Exposito, C. J. Torres, F. Herrera, J. M. Prospero, and M. C. Romero, Radiative properties of aerosols in Saharan dust outbreaks using ground-based and satellite data: Applications to radiative forcing, *J. Geophys. Res.*, *106*, 18403–18416, 2001. 3.1, 4
- Dickerson, R. R., S. Kondragunta, G. Stenchikov, K. L. Civerolo, B. G. Doddridge, and B. N. Holben, The impact of aerosols on solar ultraviolet radiation and photochemical smog, *Science*, *278*, 827–830, 1997. 1, 3.1
- Dubovik, O., B. Holben, T. F. Eck, A. Smirnov, Y. J. Kaufman, M. D. King, D. Tanré, and I. Slutsker, Variability of absorption and optical properties of key aerosol types observed in worldwide locations, *J. Atmos. Sci.*, *59*, 590–608, 2002. 3.1, 4
- Feichter, J., U. Lohmann, and I. Schult, The atmospheric sulfur cycle in ECHAM-4 and its impact on the shortwave radiation, *Climate Dynamics*, pp. 235–246, 1997. 4
- Galy-Lacaux, C., C. R. Carmichael, C. H. Song, J. P. Lacaux, H. A. Ourabi, and A. I. Modi, Heterogeneous processes involving nitrogenous compounds and Saharan dust inferred from measurements and model calculations, *J. Geophys. Res.*, *91*, 12559–12578, 2002. 1, 3.2
- Ginoux, P., Effects of non-sphericity on mineral dust modeling, *J. Geophys. Res.*, *108*, 4052, doi:10.1029/2002JD002516, 2003. 2.2
- Ginoux, P., M. Chin, I. Tegen, J. Prospero, B. Holben, O. Dubovik, and S.-J. Lin, Sources and distributions of dust aerosols simulated with the GOCART model, *J. Geophys. Res.*, *106*, 20555–20273, 2001. 2.2, 3.1, 3.3, 4
- Goodman, A. L., G. M. Underwood, and V. H. Grassian, A laboratory study of the heterogeneous reaction of nitric acid on calcium carbonate particles, *J. Geophys. Res.*, *105*, 29053–29064, 2000. 1, 3.2, 3.2
- Hänel, G., The properties of atmospheric aerosol particles as functions of the relative humidity at thermodynamic equilibrium with the surrounding moist air, *Adv. Geophys.*, *19*, 73–188, 1976. 4
- Hanson, H. P., A destabilizing bias in clear-sky atmospheric heating rate calculations. 2.1
- Hauglustaine, D. A., G. P. Brasseur, S. Walters, P. J. Rasch, J.-F. Müller, L. K. Emmons, and M. A. Carroll, MOZART, a global chemical transport model for ozone and related chemical tracers 2. Model results and evaluation, *J. Geophys. Res.*, *103*, 28291–28335, 1998. 3.3
- He, S., and G. R. Carmichael, Sensitivity of photolysis rates and ozone production in the troposphere to aerosol properties, *J. Geophys. Res.*, *104*, 26307–26324, 1999. 1, 3.1, 3.1, 3.4
- Holben et al., B. N., AERONET – a federated instrument network and data archive for aerosol characterization, *Remote Sens. Environ.*, *66*, 1–16, 1998. 3.3

- Hough, A. M., Development of a two-dimensional global tropospheric model: Model chemistry, *J. Geophys. Res.*, *96*, 7325–7362, 1991. 2.1
- Jacob, D. J., et al., Deposition of ozone to tundra, *J. Geophys. Res.*, *97*, 16473–16479, 1992. 2.1
- Jacobson, M. Z., Studying the effects of aerosols on vertical photolysis rate coefficient and temperature profiles over an urban airshed, *J. Geophys. Res.*, *103*, 10593–10604, 1998. 1, 3.1
- Karyampudi, V. M., et al., Validation of the Saharan dust plume conceptual model using lidar, Meteosat, and ECMWF data, *Bull. Am. Meteorol. Soc.*, *80*, 1045–1075, 1999. 3.2
- Kaufman, Y. J., D. Tanré, O. Dubovik, A. Karnieli, and L. A. Remer, Absorption of sunlight by dust as inferred from satellite and ground-based remote sensing, *Geophys. Res. Lett.*, *28*, 1479–1482, 2001. 3.1, 4
- Kinne, S., et al., Monthly averages of aerosol properties: A global comparison among models, satellite data and AERONET ground data, *Submitted to J. Geophys. Res.*, 2003. 1
- Kohfeld, K. E., and S. P. Harrison, DIRTMAP: The geologic record of dust, *Earth Sci. Revs.*, *54*, 81–114, 2001. 1
- Li-Jones, X., and J. M. Prospero, Variations in the size distribution of non-sea-salt sulfate aerosol in the marine boundary layer at Barbados: Impact of African dust, *J. Geophys. Res.*, *103*, 16073–16084, 1998. 4
- Li-Jones, X., H. B. Maring, and J. M. Prospero, Effect of relative humidity on light scattering by mineral dust aerosol as measured in the marine boundary layer over the tropical Atlantic Ocean, *J. Geophys. Res.*, *103*, 31113–31121, 1998. 3.1
- Liao, H., and J. H. Seinfeld, Radiative forcing by mineral dust aerosols: sensitivity to key variables, *J. Geophys. Res.*, *103*, 31637–31645, 1998. 3.1
- Liao, H., P. J. Adams, S. H. Chung, J. H. Seinfeld, L. J. Mickley, and D. J. Jacob, Interactions between tropospheric chemistry and aerosols in a unified general circulation model, *J. Geophys. Res.*, *108*, 4001, doi:10.1029/2001JD001260, 2003. 1
- Lohmann, U., J. Feichter, C. C. Chuang, and J. E. Penner, Prediction of the number of cloud droplets in the ECHAM GCM, *J. Geophys. Res.*, *104*, 9169–9198, 1999. 4
- Luo, C., N. M. Mahowald, C. S. Zender, and J. del Corral, A 22-year climatology of mineral aerosols, *Submitted to J. Geophys. Res.*, 2003. 2.2, 2.2, 4
- Mahowald, N. M., C. S. Zender, C. Luo, D. Savoie, O. Torres, and J. del Corral, Understanding the 30 year Barbados desert dust record, *J. Geophys. Res.*, *107*, 4561, doi:10.1029/2002JD002097, 2002. 2.2
- Martin, R. V., et al., Interpretation of TOMS observations of tropical tropospheric ozone with a global model and in situ observations, *J. Geophys. Res.*, *107*, 4351, doi:10.1029/2001JD001480, 2002. 1, 3.1, 2, 3.3, 10, 4
- McLinden, C. A., S. C. Olsen, B. Hannegan, O. Wild, M. J. Prather, and J. Sundet, Stratospheric ozone in 3-d models: A simple chemistry and the cross-tropopause flux, *J. Geophys. Res.*, *105*, 14653–14665, 2000. 2.1
- Michel, A. E., C. R. Usher, and V. H. Grassian, Heterogeneous and catalytic uptake of ozone on mineral oxides and dust: A Knudsen cell investigation, *Geophys. Res. Lett.*, *29*, doi:10.1029/2002GL014896, 2002. 1, 3.2, 3, 3.2, 4
- Murphy, D. M., and D. W. Fahey, An estimate of the flux of stratospheric reactive nitrogen and ozone into the troposphere, *J. Geophys. Res.*, *99*, 5325–5332, 1994. 2.1
- Olson, J., et al., Results from the Intergovernmental Panel on Climatic Change Photochemical Model Intercomparison (PhotoComp), *J. Geophys. Res.*, *102*, 5979–5991, 1997. 3.1
- Park, J. H., M. K. W. Ko, C. H. Jackman, R. A. Plumb, and K. H. Sage, Models and measurements II, *Tech. Rep. Tech. rept.*, National Aeronautics and Space Administration, Langley Research Center, Hampton, VA, 1999. 2.1
- Patterson, E. M., Optical properties of the crustal aerosol: Relation to chemical and physical characteristics, *J. Geophys. Res.*, *86*, 3236–3246, 1981. 3.1
- Penner, J. E., et al., Aerosols, their direct and indirect effects, in *Climate Change 2001: The Scientific Basis. Contribution of Working Group I to the Third Assessment Report of the Intergovernmental Panel on Climate Change*, edited by J. T. Houghton, Y. Ding, D. J. Griggs, M. Noguer, P. J. van der Linden, X. Dai, K. Maskell, and C. A. Johnson, chap. 5, pp. 291–336, Cambridge Univ. Press, Cambridge, UK, and New York, NY, USA, 2001. 1
- Prather, M. J., Numerical advection by conservation of second-order moments, *J. Geophys. Res.*, *91*, 6671–6681, 1986. 2.1
- Price, C., and D. Rind, A simple lightning parameterization for calculating global lightning distributions, *J. Geophys. Res.*, *97*, 9919–9933, 1992. 2.1
- Pruppacher, H. R., and J. D. Klett, *Microphysics of Clouds and Precipitation*, 2nd ed., Kluwer Acad. Publ., Dordrecht, Holland, 1998. 3.2
- Ram, M., and G. Koenig, Continuous dust concentration profile of pre-Holocene ice from the Greenland Ice Sheet Project 2 ice core: Dust stadials, interstadials, and the Eemian, *J. Geophys. Res.*, *102*, 26641–26648, 1997. 1
- Rasch, P. J., N. M. Mahowald, and B. E. Eaton, Representations of transport, convection, and the hydrologic cycle in chemical transport models: Implications for the modeling of short-lived and soluble species, *J. Geophys. Res.*, *102*, 28127–28138, 1997. 2.2
- Rasch, P. J., W. D. Collins, and B. E. Eaton, Understanding the Indian Ocean Experiment INDOEX aerosol distributions with an aerosol assimilation, *J. Geophys. Res.*, *106*, 7337–7355, 2001. 2.2
- Reid, J. S., et al., Comparison of size and morphological measurements of coarse mode dust particles from Africa, *J. Geophys. Res.*, *108*, 8593, doi:10.1029/2002JD002485, 2003. 4
- Rotstayn, L. D., and U. Lohmann, Simulation of the tropospheric sulfur cycle in a global model with a physically based cloud scheme, *In Press in J. Geophys. Res.*, 2003. 4
- Savoie, D. L., J. M. Prospero, S. J. Oltmans, W. C. Graustein, K. K. Turekian, J. T. Merrill, and H. Levy II, Sources of nitrate and ozone in the marine boundary layer of the tropical North Atlantic, *J. Geophys. Res.*, *97*, 11575–11589, 1992. 3.3
- Savoie, D. L., H. B. Maring, M. A. Izaguirre, T. Snowdon, and L. Custals, Ground-based measurements of aerosol chemical, physical, and optical properties during the Puerto Rico Dust Experiment (PRIDE), vol. 81, p. F44, American Geophysical Union, 2000. 3.1, 4

- Schwartz, S. E., Mass-transport considerations pertinent to aqueous phase reactions of gases in liquid-water clouds, in *Chemistry of Multiphase Atmospheric Systems*, edited by W. Jaeschke, vol. 6 of *NATO ASI Series G: Ecological Sciences*, pp. 415–471, Springer-Verlag, Berlin, 1986. 3.2, 3.2
- Seinfeld, J. H., and S. N. Pandis, *Atmospheric Chemistry and Physics*, John Wiley & Sons, New York, NY, 1997. 4
- Sokolik, I. N., D. M. Winker, G. Bergametti, D. A. Gillette, G. Carmichael, Y. J. Kaufman, L. Gomes, L. Schuetz, and J. E. Penner, Introduction to special section: Outstanding problems in quantifying the radiative impacts of mineral dust, *J. Geophys. Res.*, 106, 18015–18027, 2001. 3.1, 4
- Song, C. H., and G. R. Carmichael, A three-dimensional modeling investigation of the evolution processes of dust and sea-salt particles in east Asia, *J. Geophys. Res.*, 106, 18131–18154, 2001. 3.2
- Tabazadeh, A., M. Z. Jacobson, H. B. Singh, O. B. Toon, S. J. Lin, R. B. Chatfield, A. N. Thakur, R. W. Talbot, and J. E. Dibb, Nitric acid scavenging by mineral and biomass burning aerosols, *Geophys. Res. Lett.*, 25, 4185–4188, 1998. 1, 3.3
- Tie, X., G. Brasseur, L. Emmons, L. Horowitz, and D. Kinnison, Effects of aerosols on tropospheric oxidants: A global model study, *J. Geophys. Res.*, 106, 22931–22964, 2001. 3.2, 3.2
- Underwood, G. M., C. H. Song, M. Phadnis, G. R. Carmichael, and V. H. Grassian, Heterogeneous reactions of NO_2 and HNO_3 on oxides and mineral dust: A combined laboratory and modeling study, *J. Geophys. Res.*, 106, 18055–18066, 2001. 1, 3.2, 5, 3.2, 4
- Valero, F. P. J., S. K. Pope, B. C. Bush, Q. Nguyen, D. Marsden, R. D. Cess, A. S. Simpson-Leitner, A. Bucholtz, and P. M. Udelhofen, The absorption of solar radiation by the clear and cloudy atmosphere during the Atmospheric Radiation Measurements Enhanced Shortwave Experiments (ARESE) I and II: Observations and models, *J. Geophys. Res.*, 108, 4016, doi:10.1029/2001JD001384, 2003. 3.1
- Wang, Y., D. J. Jacob, and J. A. Logan, Global simulation of tropospheric O_3 - NO_x -hydrocarbon chemistry. 1. Model formulation, *J. Geophys. Res.*, 103, 10713–10725, 1998a. 2.1
- Wang, Y., J. A. Logan, and D. J. Jacob, Global simulation of tropospheric O_3 - NO_x -hydrocarbon chemistry. 2. Model evaluation and global ozone budget, *J. Geophys. Res.*, 103, 10727–10755, 1998b. 3.3
- Wild, O., and H. Akimoto, Intercontinental transport of ozone and its precursors in a three-dimensional global CTM, *J. Geophys. Res.*, 106, 27729–27744, 2001. 2.1
- Wild, O., and M. J. Prather, Excitation of the primary tropospheric chemical mode in a global three-dimensional model, *J. Geophys. Res.*, 105, 24647–24660, 2000. 2.1
- Wild, O., X. Zhu, and M. Prather, Fast-J: Accurate simulation of in- and below-cloud photolysis in tropospheric chemical models, *J. Atmos. Chem.*, 37, 245–282, 2000. 2.1, 3.1
- Woodward, S., Modeling the atmospheric lifecycle and radiative impact of mineral dust in the Hadley Centre climate model, *J. Geophys. Res.*, 106, 18155–18166, 2001. 4
- Zender, C. S., H. Bian, and D. Newman, Mineral Dust Entrainment And Deposition (DEAD) model: Description and 1990s dust climatology, *J. Geophys. Res.*, 108, 4416, doi:10.1029/2002JD002775, 2003. 2.2, 2.2, 3.1, 3.2, 3.3, 3.3, 3.4, 4
- Zhang, Y., and G. R. Carmichael, The role of mineral aerosol in tropospheric chemistry in East Asia—a model study, *J. Appl. Meteorol.*, 38, 353–366, 1999. 1, 3.2, 6, 3.2, 3.2, 4
- Zhang, Y., Y. Sunwoo, V. Kotamarthi, and G. R. Carmichael, Photochemical oxidant processes in the presence of dust: An evaluation of the impact of dust on particulate nitrate and ozone formation, *J. Appl. Meteorol.*, 33, 813–824, 1994. 1, 3.3

H. Bian, C. S. Zender, Department of Earth System Science, University of California, Irvine, CA 92697-3100. (hbian@uci.edu)

Received 5 November 2002; revised 24 April 2003; accepted 2 May 2003.

This preprint was prepared with AGU's \LaTeX macros v5.01, with the extension package 'AGU++' by P. W. Daly, version 1.6b from 1999/08/19.